Amphiphilic Character and Aggregation Properties of Small Cholesterol Islands on Water: A Simulation Study

S. R. T. Cromie, M. G. Del Pópolo, and P. Ballone*

Queen's University Belfast, Atomistic Simulation Centre, Belfast BT7 1NN, United Kingdom

Received: September 24, 2008; Revised Manuscript Received: January 20, 2009

Small cholesterol clusters (Ch_n, $1 \leq n \leq 10$) on water have been investigated by molecular dynamics simulations based on an empirical force field potential. The simulation results for clusters of increasing size highlight the processes that take place during the initial stages of cholesterol aggregation at low coverage. Our results show that at $T = 280$ K clusters form spontaneously out of a dilute two-dimensional (2D) vapor of cholesterol molecules, driven by entropy and potential energy. Up to $n = 10$, corresponding to 25% coverage for our simulation cell, cholesterol molecules lay flat on the water surface, forming fluid-like 2D aggregates. Within each island, the elongated cholesterol molecules align their longest axis along a common direction, anticipating the liquid-crystal character of bulk phases. With increasing cluster size, the adsorption energy per molecule quickly saturates to a value close to the limiting value for a full monolayer coverage. Cholesterol adsorption locally changes the electrostatic surface polarization of water, giving rise to an induced moment that tends to compensate the dipole of the adsorbed island. Computations for a single cholesterol molecule and dimer in bulk water are reported for a comparison. The absorption energy of both species in bulk water is larger than their adsorption energy at the water surface, thus pointing to entropy as the origin of the amphiphilic character of cholesterol.

I. Introduction

The self-organization of amphiphile molecules in a water environment is arguably the most apparent example of complex behavior emerging from simple ingredients.[1,2] Vesicles, micelles, and bilayers are among the characteristic structures found in amphiphile−water mixtures[3] and play an important role in a vast variety of natural and man-made systems. Bilayers, in particular, are the basic structural motif of biomembranes, that, in turn, represent an essential component of every living cell.[4,5]

The investigation of the phase diagram of these remarkable systems and the analysis of their aggregation states nowadays represents a major interdisciplinary research area, stretching across physics, chemistry, and biology. The long-term goal of many such studies is to clarify and quantify the fundamental properties of biomembranes, whose variety and complexity still prevent a comprehensive description in terms of a few physical or chemical parameters. As an intermediate step, the investigation of simplified model systems provides an effective strategy to approach the final goal. Films made of a single layer of amphiphile molecules,[6] in particular, can be prepared by standard experimental techniques, and their aggregation state can be varied by changing a single thermodynamic parameter, that is, the lateral pressure Π_L (See Figure 1 and ref 1). Moreover, and despite their tenuous appearance, the properties of thin amphiphile films on water display a remarkable degree of reproducibility that, in turn, provides the basis for a growing number of applications, including sensing technology,[7] energy conversion,[8] and electronic devices.[9]

Although the experimental investigation of these organic overlayers on water has a long and distinguished history,[6] their computational analysis is far more recent but is rapidly providing a wealth of microscopic information[10] that sometimes is lacking in experimental results. Because of inherent interest and computational convenience, computer simulations have been restricted in most cases to high coverage systems. Moreover, and again for computational convenience, many simulations have been based on implicit solvent models,[11] replacing water with an external, anisotropic potential acting on the adsorbed organic molecules. However, crucial stages in the amphiphile self-organization, such as the nucleation of an ordered overlayer, take place at low coverage, and the detailed description of the water−molecules interaction is required to provide a reliable description of these rate-limiting steps.

To enhance our understanding of these and closely related issues, we carried out an extensive computational investigation of small cholesterol clusters (Ch_n, $1 \leq n \leq 10$) adsorbed on the water surface at near ambient temperature ($T = 280$ K), using molecular dynamics and an empirical, rigid ion force field. Simulations of the single molecule and dimer absorbed in bulk water have been carried out as well to provide a framework to gauge the adsorption results. The immediate aim of our investigation is to clarify the role of water mediated interactions among adsorbed cholesterol molecules and to explore the relative stability of potential nucleation centers for the formation of condensed overlayers.

Cholesterol is a well-known lipid of moderate complexity, which represents a minority yet essential component of cellular membranes, that in addition contain a significant amount of phospholipids and also a variable but often sizable concentration of proteins.[5] Moreover, cholesterol forms pure[12] and monohydrate[13] crystals whose structure has been determined by X-ray diffraction. In the solid phase it is the major constituent of several biomaterials, including the basic component of gallstones.[14]

Several chemical variants of the basic cholesterol molecule are known, such as, for instance, ergosterol, lanosterol, and desmosterol. A few of these variants differ from cholesterol only

* Corresponding author. Phone: +44 (2890) 975329; e-mail: p.ballone@qub.ac.uk.

10.1021/jp8084759 CCC: $40.75
Published on Web 03/10/2009

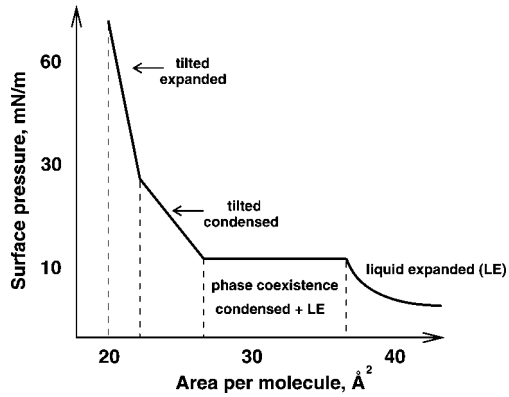

Figure 1. Schematic drawing of a Langmuir isotherm.

by minor structural details, but nevertheless display rather different chemical-physics properties and are preferentially incorporated into membranes specialized to carry out different tasks. This selectivity emphasizes the uniqueness and importance of the role that cholesterol plays in living cells, perhaps regulating the overall membrane fluidity.[15] Moreover, together with sphingolipids, cholesterol is an essential component of lipid rafts,[16] that is, microdomains in the liquid ordered phase of biomembranes that provide the location of choice for the absorption and for the activity of several transmembrane proteins.

Neutron diffraction studies show that in the most common phospholipid bilayers cholesterol is incorporated in an upright geometry, with its hydroxyl termination in contact with water.[17] Recent experimental results,[18] however, show that in disordered, poly-unsaturated lipid membranes, cholesterol might preferentially reside between the two phospholipid layers, far from the organic−water interface. If confirmed, these results suggest that the inclusion and activity of cholesterol in natural and artificial membranes might not always depend on its amphiphilic character. The nucleation of cholesterol crystals out of a water environment, however, does strictly depend on this property.

Cholesterol thin films on water have recently been prepared using a relatively standard inverse Langmuir technique and have been characterized by grazing incidence X-ray diffraction.[19] The results document the progressive formation of an ordered monolayer on water and the successive growth of a multilayer structure. Because of intrinsic limitations of the experimental technique, no information is provided for coverages significantly below the full monolayer. In many respects, our investigation aims at extending the description of cholesterol aggregation on water down to coverages that were, up to now, inaccessible to standard experimental approaches. Moreover, our results will provide a quantitative base for tuning coarse graining models.[21]

In what follows we first describe the model and the simulation method, then we present and discuss the results of our investigation for the absorbed and adsorbed cholesterol clusters. Our results show that aggregation on the water surface takes place spontaneously, driven by entropy and potential energy. The resulting cholesterol islands behave as 2D liquid crystal droplets, in which cholesterol molecules lay flat on the water surface, orienting their longest molecular axis along a common direction. The translational disorder and molecular mobility are remarkable at a temperature ($T = 280$K) far below the melting temperature ($T_M = 422.3$ K, see ref 22) of bulk cholesterol, apparently due to both the nanometric size of the clusters and to their interaction with the water surface, giving rise to a 2D growth mode.

The present study is the first stage of a long-term investigation of a variety of 2D and 3D cholesterol phases.

II. The Model and the Simulation Method

The relevance of a classical simulation study strictly depends on the accuracy and reliability of the underlying model potential. Empirical potentials for hydrocarbon and their simplest derivatives such as monovalent alcohols are well developed and have been successfully used in simulations. The most popular potentials[23] consist of the sum of bonded and nonbonded interactions, the former including stretching, bending, and torsion energy terms, with the latter accounting for electrostatic and dispersion energy contributions. Most of these models do not explicitly describe effects due to the polarizability of the electron density, even though part of the energy contributions arising from polarization is often folded into the short- and long-range nonbonded interactions. This folding procedure, however, limits the validity range of the potential to systems such that the local environment around each molecule is similar to the one assumed in the potential construction stage, which may lead to sizable errors whenever the molecule is investigated within an environment of different bonding character and/or polarity. Water itself is one of the most thoroughly investigated systems, and simple classical potentials, although far from perfect, provide a robust description of this all important molecular fluid.[24]

The cholesterol (Ch) molecule consists of an OH apex, a rigid polycyclic body, and a flexible alkane tail (see Figure 2). Two methyl groups (M1 and M2 in Figure 2) sticking out of the same side of the polycyclic body (β-side, as opposed to the flat α-side) break the approximately planar symmetry of the Ch molecule. The intramolecular backbone of covalent bonds appears to be nearly free of strain, apart from a slight distortion of the 5-fold ring $C_{13}-...-C_{17}$, and an even smaller deformation of the $C_5-...-C_{10}$ 6-fold ring due to the double bond between C_5 and C_6. The electronic polarizability of cholesterol is relatively small (especially considering the molecular size), as shown by the low value of the high frequency dielectric constant ($\varepsilon_\infty \approx 2$) for liquid and solid phases of cholesterol and closely related derivatives.[25] Computations performed using the Perdew-Burke-Ernzerhof (PBE, see ref 26) exchange-correlation approximation in the Siesta implementation[27] show that the hydrogen bonding (HB) of cholesterol with water is of moderate strength, with a slight advantage for cholesterol accepting an HB (binding energy $E_{HB}^{(a)} = 8.17$ kcal/mol) with respect to the complementary combination in which cholesterol is the donor (binding energy $E_{HB}^{(d)} = 7.26$ kcal/mol). All those properties are typical of relatively inert and well behaved organic systems; therefore, it could be expected that several of the available generic force fields might reproduce well the properties of this molecule. Moreover, specific models for cholesterol[28] have been developed and validated, providing satisfactory results for a variety of properties that include structural and cohesive energies of solids.

Despite the availability of a specific, well tuned potential, we decided to build our own cholesterol model adopting the Amber functional form,[29] tuning the force field parameters on density functional (DF) results for the gas phase molecule, and experimental data for the crystal phases.[12,13] Density functional data for the hydrogen bonding of cholesterol and water are also included into the database. The Amber functional form, somewhat simpler than the form used in ref 28, has the advantage of being compatible with most simulation packages, including the DL-POLY program (see ref 30) used for most of

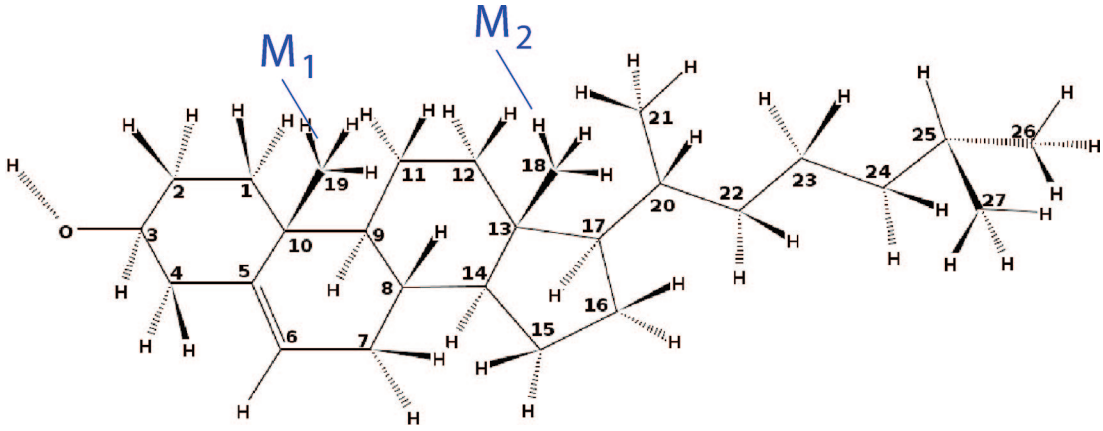

Figure 2. Schematic drawing of cholesterol.

our computations. The slight loss of accuracy caused by the simplification of the analytic form is to a large extent compensated by a slight increase in the number of atom types. The detailed comparison of our model with that of ref 28 shows that the two potentials are virtually equivalent.

Our potential energy, therefore, will consist of intra- and intermolecular terms. The former, in turn, consist of stretching, bending, and dihedral terms. The latter consist of Coulomb forces, described in terms of fixed atomic charges, and dispersion terms, approximated by the 6 − 12 Lennard−Jones (LJ) potential. At variance from the potential of ref 28, no Urey−Bradley term is included in our model.

Vibrational frequencies and eigenvectors obtained from DF (Siesta) computations allow a detailed tuning of the intramolecular force field parameters. In addition, atomic charges can be obtained by fitting the electrostatic potential around the gas-phase cholesterol molecule as given by DF computations for the ground state. These so-called electrostatic potential (ESP) charges underly several of the most popular force field models. The dipole moment of the gas-phase ground-state structure turns out to be 5.75 debye, which is relatively small for a 74 atom molecule. In the ground-state structure this dipole is predominantly located at the OH termination, but its precise orientation and value depend on the configuration of the molecular tail, even though the polarity of this alkane moiety is low.

The LJ potential, however, cannot be fully and independently determined by the available data, consisting mainly of the experimental results for the crystal density and equilibrium atomic positions. For this reason, in the first instance, we adopted the same LJ parameters of the force field developed in ref 28. As already mentioned in the introduction, two crystal forms are known for pure cholesterol,[12] and a monohydrate crystal has been characterized as well.[13] We verified that without further fitting the force field reproduces fairly well the volume of all these to within 2% and also that the atomic positions obtained by relaxing the crystallography data do not deviate much from the input positions, that, moreover, are affected by sizable uncertainties because of residual disorder at the cholesterol tail in the crystal. We note that the LJ energy parameters (ε) for the hydrocarbon atoms are systematically larger than in other potentials extensively used to simulate similar materials.[31] This observation, however, is only marginally relevant, since bonding properties are determined by the combination of Coulomb and dispersion terms, and in ref 28 their sum has been tuned and then verified on properties of the solid phases.

In our simulations water is described by a flexible 3-center potential (SPC/Fw, see ref 32), whose properties have been thoroughly investigated. All these considerations together suggest that the potential for the pure components, that is, cholesterol and water, is relatively under control and is expected to provide a fair description of each of these two materials.

The cross interaction between cholesterol and water, however, represents a relatively unknown ingredient, which significantly affects the simulation results. Once again, the most uncertain contribution is that of dispersion interactions. Hydrogen bonding, for instance, in our model is largely (if not exclusively) dependent on Coulomb forces, determined in turn by the ESP charges and atomic radii. Dispersion forces, instead, are not readily available from ab initio computations,[33] therefore their strength for water interacting with carbon atoms and hydrogens in the hydrocarbon body and tail of cholesterol is still largely underdetermined.

The simplest choice for the cholesterol−water LJ parameters (ε, σ) is based on the well-known ideal mixing rules (Berthelot rules). The results of preliminary but extensive simulations, however, pointed to a significant overestimation of the water−cholesterol attraction, resulting in the incorporation of cholesterol below the water surface. More importantly, experimental measurements show that cholesterol forms ordered single-, bi-, and multilayer structures on the water surface.[19] The stability of these systems was not reproduced by simulation, which instead quickly evolved toward highly disordered and partially mixed water/cholesterol structures. The experimental picture, however, could be reproduced by decreasing the water−cholesterol dispersion interaction. The reduction was enforced by rescaling the ε values for the cross interactions by a fixed factor, thus overriding Berthelot's rules, and settling for the minimum rescaling able to restore the stability of the ordered cholesterol overlayers. More precisely, we applied a 25% reduction in the (water-O)−C interaction, and we reduced the strength of the (water-O)−(cholesterol H) interaction by 20%. The full set of parameters defining our force field is listed in the accompanying Supporting Information.

A visual account of the importance of the cross interaction rescaling is given in (Figure 3), displaying the equilibrium position of a cholesterol molecule at the surface of a water slab, under the constraint that the molecule axis (identified with the C−C vector) is perpendicular to the free surface of the water slab.

The reduction of the LJ parameters described above does not affect the strength of the water−cholesterol hydrogen bonding, since in our model the LJ ε values of the O···H nonbonded interaction is identically zero for the O−H···O combination. Nevertheless, the strength of this particular bond is somewhat

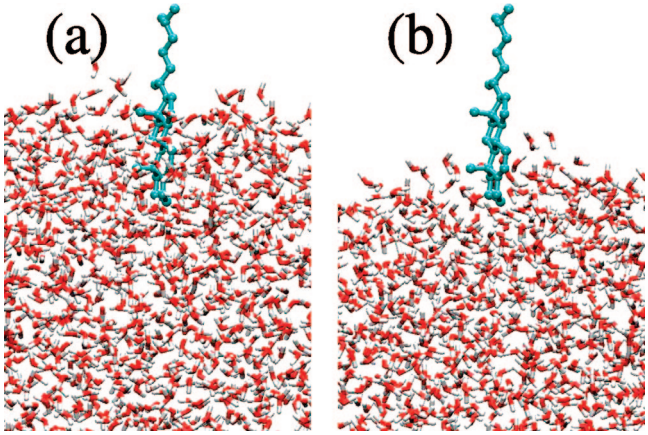

Figure 3. Equilibrium position before and after the rescaling of the water−cholesterol dispersion interactions (see text). A constraint has been added to keep the long molecular axis parallel to the z-direction.

underestimated by our potential, predicting a cohesive energy $E_{HB}^{(d)} = 5.29$ kcal/mol for the cholesterol (donor)−water (acceptor) hydrogen bond, to be compared with the $E_{HB}^{(d)} = 7.26$ kcal/mol given by DF-Siesta. Moreover, the model gives $E_{HB}^{(a)} = 5.37$ kcal/mol for the water (donor)−cholesterol (acceptor) combination, instead of $E^{(a)} = 8.17$ kcal/mol again computed by DF-Siesta. Despite the crucial role of HB for our study, we accept this discrepancy since we found indications that the Siesta implementation, together with our choice of computational parameters, slightly overestimates the cohesive energy of hydrogen bonds. For instance, the cohesive energy of the water dimer predicted by Siesta is $E_c = 6.8$ kcal/mol, whereas benchmark PBE computations give $E_c = 5.07$ kcal/mol (see ref 34), and the experimental estimate is $E_c = 5.4 \pm 0.7$ kcal/mol.[35] The observed discrepancy between the empirical force field and the ab initio result, therefore, might in fact compensate for inaccuracies in the DF data caused by computational approximations in our Siesta computations.

Molecular dynamics simulations have been performed using the DL-POLY package. Runs for all samples consisting of a slab limited by two parallel, planar surfaces have been carried out in the NVT ensemble, with a time step of 0.001 ps. Equilibration runs lasted at least 1 ns and often for several nanoseconds. Statistics have been accumulated over runs of 5−10 ns. For each system, in particular, we verified by linear interpolation that the time dependence of fluctuating quantities such as potential and kinetic energy do not drift in time during production runs.

The time scale of our simulations is fairly short compared to the relaxation times expected for compact layers of an organic molecule of the cholesterol size and complexity, and long rotational reorientation times (up to 0.6 ns for coumarin on water) have been measured experimentally for organic molecules of similar size on water.[36] However, as shown by the estimated error bars listed below, our simulation times appear to be sufficient for the relatively open structures and fairly high molecular mobility of the adsorbed clusters. The good equilibration of our systems and the convergence of our results is also supported by the fact that, during our simulations and for every cluster size, we observe several isomerization events in the geometry of the Ch islands, showing that their structure is not kinetically frozen into a single minimum of the potential energy surface. This observation is particularly remarkable, given the fact that bulk cholesterol is solid at the temperature of our simulations. The relatively quick isomerization rate is likely to be due partly to the small size of the Ch islands and partly to the interaction with water.

Simulations of similar length for system of equivalent size have been carried out in the NPT ensemble ($P = 1$ atm) to compute properties of bulk water, and to investigate bulk absorption properties of a single cholesterol molecule and Ch_2 dimer in water.

On average, molecular dynamics simulations covering 1 ns required 4 days of computation on 8 nodes of a 64 bit OPTERON computer.

III. Simulation Results

A. Bulk Water and the Water Slab. In a first stage of our study, we carried out NPT simulations of bulk water, represented by $N_w = 2850$ molecules in a cubic box periodically repeated in space. At $T = 280$ K and $P = 1$ atm, the average density turns out to be $\rho_w = 1.019$ g/cm^3, and the diffusion constant of water molecules is estimated at $D = 2.35 \pm 0.05 \times 10^{-5}$ cm^2/s, in good agreement with the results of ref 32 for the same potential.[37]

Next, we characterized the properties of the clean water surface. In our computations this is represented by a slab of $N_w = 2850$ water molecules, periodically repeated in space, with a large gap ($\Delta \approx 110$ Å) separating replicas in the direction (z) perpendicular to the surface. The analysis of the pure water surface has been carried out on a slab of 1525 Å^2 surface area and $W \approx 0$ 56 Å thickness (the actual periodicity in the z direction is $\Delta + W = 170$ Å), which guarantees a fair decoupling of the two slab surfaces. The target temperature of our NVT simulations was set to 280 K. Statistics have been accumulated over 5.0 ns, after a 1 ns equilibration.

The surface tension has been computed using the definition:

$$\gamma = \int_{in}^{out} [\Pi_\perp - \Pi_{||}]dz \qquad (1)$$

where $\Pi_\perp$ and $\Pi_{||}$ are the normal and parallel components of the pressure tensor across the interface,[39] and the integral extends from a point well inside the water slab (in) to a point on the vapor side of the interface (out). Mechanical stability requires $\Pi_\perp$ to be constant over the entire system, and variations of the parallel component $\Pi_{||}$ at the interface are directly related to the surface tension. In the case of our water slab, the computed surface tension turns out to be $\gamma_w = 62 \pm 4$ mJ/m^2, in line with the results obtained using similar empirical water models[40] but still significantly lower than the experimental value $\gamma_w = 74.6$ mJ/m^2 at $T = 280$ K.[41]

The density profile for hydrogen extends slightly beyond that of oxygen, suggesting that the outermost surface layer is preferentially populated by H atoms. Despite this (slight) prevalence of positive charge in the tail of the density distribution, the average dipole polarization at the surface is directed from the outside to the inside of the water slab.[42] The net polarization of each surface, however, is fairly small, only amounting to 0.0076 ± 0.0006 debye/Å^2, corresponding to an average dipole of 0.3 debye for the area ($A_1 \approx 38$ Å^2) covered by an upright cholesterol molecule in the ordered mono- and bilayer structures.[19] This low dipole polarization is likely to play a correspondingly small role in the determination of the interfacial properties, even though the long-range and intrinsic strength of dipole−dipole interactions may still give rise to surprises.

Convergence of the surface properties with respect to the slab size have been verified by comparison with the results obtained

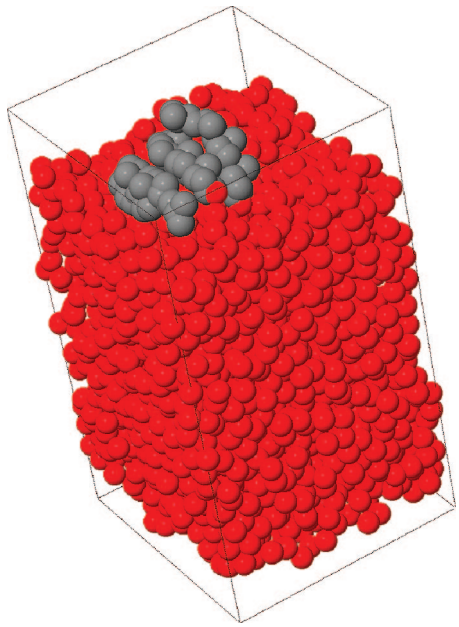

Figure 4. Snapshots of the simulation cell for Ch_3/water. Only non-hydrogen atoms are shown.

for a smaller system size ($N_w = 1432$ water molecules and 1014 Å^2 cross area). The surface properties of this second slab are the same as those computed for the $N_w = 2850$ sample to within the estimated error bar.

Two different slab geometries have been used for the cholesterol clusters on water simulations. The first one coincides with the one described above, having a cross area of 1525 Å^2, and used for clusters of up to $n = 5$ cholesterol molecules. The second one has an area of 1802 Å^2, and was used for the $n = 6$, 7, and 10 simulations. Despite the slight advantage in area, even this larger slab is not sufficient to confine the $n = 10$ cluster, which gives rise to a connected structure (stripe) extending across the simulated water surface. Because this last geometry has its own reasons of interest, we did not repeat the $n = 10$ simulation with a slab of wider area, as it would have been possible from the computational point of view. A first visual impression of the size of the systems we simulated can be obtained from Figure 4. It is apparent that the distance of periodic images is not much larger than the longitudinal dimension of the cholesterol molecule. It is, however, much longer than the atomic (van der Waals) radii, which in fact determine the range of dispersion forces. Coulomb interactions among periodic replicas are expected to be fairly small, since cholesterol is neutral, and its polarity is modest. Other interactions are certainly present, such as those mediated by capillary waves, whose range may be longer than the simulation cell periodicity (see ref 43). However, simulations for Ch_6 islands on water carried out on the two slabs of different surface area described above gave results that differ by less than the statistical error bar.

B. Single Cholesterol Molecule and Dimer in Bulk Water. The properties of a single cholesterol molecule in water have been investigated to provide a comparison for the properties of cholesterol aggregates on water. Cholesterol, in fact, is nearly insoluble in water, and measuring its properties in homogeneous water−cholesterol mixtures might be impossible in reality. Even the quantitative determination of solubility is affected by large experimental errors, being estimated at 0.47×10^{-8} g/(mol ml) in ref 44 ($T = 298$ K), and at 2.2×10^{-8} g/(mol ml) in ref 45 ($T = 303$ K). Simulation, however, allows us to perform this computational experiment, the results of which aided our understanding of the properties of cholesterol overlayers on water. A sample of 2850 water molecules and 1 Ch enclosed in a cubic box has been simulated in the NPT ensemble at $T = 280$ K and $P = 1$ atm. Equilibration lasted 1 ns, and statistics have been collected over an additional run of 6 ns.

The absorption energy E_{abs} of cholesterol *in* water, determined according to the usual definition:

$$E_{abs} = -\{U[\text{Ch in water}] - U[\text{water}] - U[\text{Ch}]\} \quad (2)$$

turns out to be 27 ± 4 kcal/mol. In the equation above, U[Ch + water] is the average potential energy at $T = 280$ K of the [Ch in water] sample, U[water] is the corresponding average for a bulk water sample of the same size and thermodynamic condition, and U[Ch] is the average potential energy of a gas-phase cholesterol molecule at the same temperature. The relatively large error bar on E_{abs} is due to the fact that the difference of two large fluctuating quantities (U[Ch in water] and U[water]) appears in its definition. Although fairly small, the computed value for E_{abs} is not negligible and might appear in conflict with the idea of cholesterol as a predominantly hydrophobic species. However, as briefly mentioned below and extensively discussed in the literature, hydrophobicity is never due to a repulsive water−guest interaction but arises from the competition with more stable phases and from entropy effects in the surrounding water layer.[46−49] The analysis of the different energy contributions shows that the cross water−cholesterol Coulomb and dispersion interactions are the primary sources of cohesion,[50] accounting for a ∼40 kcal/mol decrease of the average potential energy, only partially compensated by a slight increase (∼15 kcal/mol) of the water−water average potential energy, apparently due to the distortion of the water hydrogen bonding network. The cholesterol intramolecular energy is nearly unchanged upon absorption, with only a minor energy increase that, however, is comparable to the error bar of the energy estimates.

Experiments[22] and computations performed with the present Ch potential agree in their prediction of $E_{coh} = 40.2$ kcal/mol for the cohesive energy of the equilibrium crystal phase of cholesterol at $T = 280$ K. A quick order-of-magnitude estimate shows that the model reproduces semiquantitatively the low solubility of cholesterol in water. The estimate, however, neglects the role of entropy, which is expected to be fairly important, as shown by experimental and computational investigations of hydrophobic solvation.[51,52] The unknown size of this free energy contribution, which is difficult to estimate by simulation, together with the large experimental uncertainties prevents us from using the experimental value of solubility for an accurate determination of the water−cholesterol cross interactions. Moreover, the quantitative determination of solubility requires accounting for all the different forms possibly in equilibrium with the homogeneous solution, including the cholesterol hydrate crystals and all heterogeneous phases such as vesicles, micelles, etc.

The near invariance of the cholesterol intramolecular energy in going from the gas to the solvated phase is consistent with the fact that absorption changes only slightly the shape and size of Ch, as measured, for instance, by the molecule principal momenta of inertia. The elongated shape of Ch gives rise to two large and nearly equivalent components ($I_2 \approx I_1$) of the (diagonal) inertia tensor and to a single smaller component ($I_3 \ll I_2 \approx I_1$), corresponding to rotations around the long molecular axis. These geometrical properties provide the basis for the

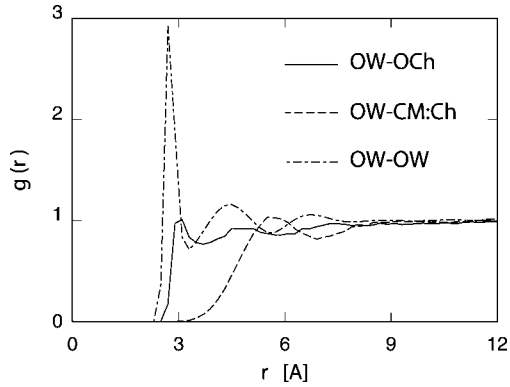

Figure 5. Radial distribution functions for a single cholesterol molecule in bulk water. Radial distances are computed from the cholesterol center of mass (CM:Ch), the apical oxygen of cholesterol (O:Ch), and the oxygen atoms of water (OW), as indicated in the figure.

simplest coarse graining model for cholesterol, representing the molecule as a prolate ellipsoid. In the gas phase, the isomerization dynamics of the Ch molecule (simulated for a few nanoseconds at $T = 280$ K) somewhat broadens the probability distribution for the momenta of inertia, without significantly changing the basic picture provided by the ground-state geometry. Immersion in water slows down the isomerization dynamics, as described in some more detail in the following subsection, and partly reverses the thermal broadening of the probability distribution for the Ch inertia moments. In all cases, however, the changes in the average value of the inertia momenta due to thermal motion and/or absorption are fairly small.

The distribution of water molecules around cholesterol has been characterized by computing the radial distribution function (see Figure 5) of water oxygen (OW) around: (i) the Ch center of mass (CM:Ch), and (ii) around the Ch oxygen (O:Ch). Surprisingly, even the CM:Ch-OW radial distribution shows a broad but clear first peak, although the elongated geometry of cholesterol is expected to give rise to a fairly wide range of closest approach distances. Nevertheless, Figure 5 suggests that the OW density in the vicinity of cholesterol is less than in bulk water, possibly because of the hydrophobic character of the Ch main body. The OW depletion, in particular, might be attributed to the water tendency to form a low-energy, low density interface around Ch by strengthening water−water hydrogen bonds at the expense of water−solute interactions. This effect is apparent even in the distribution of OW around the hydrophilic OH termination of Ch, as shown by comparison with the OW−OW radial distribution function, also displayed in Figure 5.

The decrease of the water density in its vicinity, possibly due to the competing role of the water−water bonding, is the most likely responsible for the fairly low number of hydrogen bonds that cholesterol forms with water. As expected, the OH termination of cholesterol participates in hydrogen bonding both as a donor (d) and as an acceptor (a). In our model, hydrogen bonds can be identified by geometric parameters only. In what follows, we define hydrogen bonds as the combination of three atoms O−H−O such that the O−O distance is less than 3.5 Å, and the ∠OHO angle deviates less than 30° from linearity. The analysis of simulation trajectories for the single Ch molecule on water shows that at any given time the probability of finding the OH termination of cholesterol engaged in a HB as a donor is 64%, whereas the probability of cholesterol receiving at least one (a)-bond is 88%. Moreover, in most cases only one accepted HB is present, the probability of accepting two bonds at the same time is only 14%, resulting into an average number of accepting bonds equal to 1.02. Taking into account the number of donating (one) and accepting (two) HB that can be formed by Ch, the ratio of these probabilities implies that, at variance from the static Ch−H_2O case reported in Section II, the donating bond of Ch is somewhat more stable than the corresponding accepting bonds. More importantly, the relatively low equilibrium population of either accepting or donating bonds implies that geometry constraints and competing water−water interactions reduce the thermodynamic stability of the Ch−water hydrogen bonding, which, on the basis of potential energy alone ($E_{coh} \approx 8$ kcal/mol at the DF level, and $E_{coh} \approx 5.5$kcal/mol according to our potential), could be expected to be fully saturated at $T = 280$ K.

The real-time dynamics of the H-bonding of cholesterol is quantified by first identifying the oxygen and hydrogen atoms linked at any given time τ and then computing the probability $P(t)$ of finding them still bonded after a time t. The analysis of trajectories shows that, because of thermal motion, hydrogen bonds break easily and quickly on a time scale of less that 1 ps, but often they reform among the same atoms within an equally short time. Only on a longer time scale (a few picoseconds), dictated by diffusional motion, do the oxygen atoms appear to change HB partners on a more permanent basis. The distinction of these two dynamical processes has been pointed out several times in the literature (see, for instance, ref 53), eventually motivating a more refined definition of HB.[54] We retain the simplest definition in our analysis, based on distances and angles, but we consider bonds that break but reform within a picosecond as intact. In this way we emphasize the role of the long time scale (diffusive) component of the HB dynamics, and we neglect the high frequency vibrations of OH, which, in any case, are only poorly represented by the classical mechanics picture underlying molecular dynamics. The time dependence of $P(t)$ is exponential ($P(t) = P(0)\exp[-t/\tau_0]$) both for accepting and donating bonds, consistent with the idea that breaking a hydrogen bond is an activated process. A slight anomaly is barely visible at times shorter than 1 ps, possibly due to our smoothing of the high frequency effects. For a single Ch molecule in water the time constant τ_0 is 5.0 ps for donating bonds and 5.6 ps for accepting bonds, suggesting that the barrier to break/form accepting or donating bonds is nearly the same.[55] Similar time constants τ_0 have been obtained in ref 32 for the HB dynamics of water using the same SPC/Fw potential. In that case, of course, the accepting and donating character are complementary definitions of the same bonds, and the time constants for their breaking and formation are by necessity the same. Moreover, experimental measurements provide again very similar values for the lifetime of hydrogen bonds in small water clusters,[56] suggesting that the time constants estimated in our simulations are primarily determined by the surface water dynamics. Much longer time scales are estimated by experiments and by simulations for highly hydrophilic organic and biological solutes.[57]

The diffusion constant of cholesterol in water has been computed from the time dependence of the mean square displacement of the Ch center of mass (R_{CM}) according to the well-known Einstein's relation:

$$D = \frac{1}{2d}\lim_{t\to\infty}\frac{\langle |R_{CM}(\tau + t) - R_{CM}(\tau)|^2\rangle_\tau}{t} \qquad (3)$$

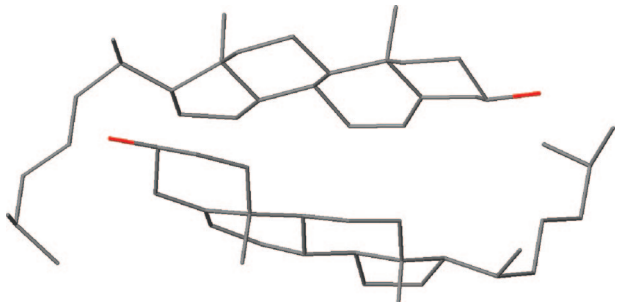

Figure 6. Ground state geometry of the gas-phase Ch_2 cluster. Only non-hydrogen atoms are shown.

where d is the dimensionality of the random walk (i.e., $d = 3$ for bulk diffusion, and $d = 2$ for diffusion on a surface), and $\langle ... \rangle_\tau$ indicates averaging with respect to the initial time τ. The average slope of $\langle |R_{CM}(\tau + t) - R_{CM}(\tau)|^2 \rangle_\tau$ versus t for $0.5 \leq t \leq 1$ ns has been used to estimate D, which turns out to be $D = 0.32 \pm 0.1 \times 10^{-5}$ cm^2/s at the temperature $T = 280$ K of our simulation.

Besides diffusion, the dynamics of the Ch molecule in water includes rotations and fairly rare isomerization processes of the alkane tail. To some extent, these last two types of motion are reflected in the time evolution of the electrostatic dipole moment, computed from the partial charges entering the definition of the interatomic potential. The Ch dipole moment tends to be of nearly constant length ($|P_{Ch}| = 5.56 \pm 0.02$ debye) but shows rapid variations in orientation. The time dependence of the dipole autocorrelation function is not exponential but displays at least two different time scales, that is, a short one of ~1 to 2 ps, possibly due to fast vibrational motion, and a longer relaxation time of ~50 ps, probably related to rotations and isomerization processes.

Two Ch molecules in bulk water have been simulated under the same thermodynamic conditions of the single molecule for 5 ns following a 1 ns equilibration run. The results show that the two Ch molecules form a stable aggregate. The relative position of the two molecules displays large amplitude fluctuations, but their relative orientation is fairly constant and corresponds to that of the Ch dimer in the gas phase at the same temperature (see Figure 6).

The absorption energy of the Ch_2 cluster amounts to 34 ± 4 kcal/mol, or 17 ± 4 kcal/mol per molecule, that is, much less than the 27 ± 4 kcal/mol absorption energy estimated for the single cholesterol molecule in water. This result, together with the apparent stability of the Ch_2 dimer in water, points to entropy as the origin of aggregation. However, the translational entropy of cholesterol is reduced by aggregation, whereas the vibrational properties appear to be only slightly affected both by solvation and by cholesterol aggregation in water. Therefore, the entropy increase driving the aggregation of Ch_2 has to be attributed to water. These conclusions are strengthened by comparison with the gas phase results, predicting a 15 kcal/mol binding energy for Ch_2 at $T = 280$ K.

No Ch−Ch hydrogen bonding is observed in our simulations for Ch_2 in water, as could have been expected from the predominant geometry shown in Figure 6. Moreover, the properties of the Ch−water hydrogen bonding are indistinguishable from those of the single Ch case. The average dipole moment of the Ch dimer in water is 3.62 ± 0.06 debye, and the average dipole moment of each individual molecule is 5.38 ± 0.02 debye, that is, very similar to that of the Ch monomer at $T = 280$ K, either in water or in the gas phase. These results show that the two molecular dipoles tend to partially compensate each other, again consistent with the dimer geometry of Figure 6.

C. Cholesterol Adsorption on Water: The Monomer and the Dimer. Small cholesterol islands (Ch_n, $n = 1, 2, 3, 4, 5, 6, 7$, and 10) on water have been simulated to quantify adsorption properties at low coverage and to investigate the Ch−Ch aggregation processes that take place when the lateral pressure Π_L is progressively increased from the vapor side of the Langmuir−Blodgett phase diagram. All simulations have been performed at $T = 280$ K in the NVT ensemble.

The first simulation concerns a single molecule deposited on a water slab of 1525 Å^2 cross area. The system has been equilibrated for 3 ns, and statistics have been accumulated during a second run of 10 ns duration.

The adsorption energy is estimated to be $E_{ads} = 14 \pm 4$ kcal/mol (see eq 4 below for its precise definition), more than half of which (8 kcal/mol) is due to short-range dispersion interactions, and the remaining part is due to hydrogen bonding. Even though the large error bars may blur the fine details in the energetics of sorption, the simulation results show that the adsorption energy of cholesterol on water is much less than the absorption energy in water. Moreover, the translational entropy favors the solvated state over adsorption confined to the surface. Nevertheless, the preference of cholesterol for the water surface is apparent both in experiments and in our simulations. Once again, entropy variations are the only conceivable reason for this behavior, and arguments similar to those discussed in the previous section imply that these variations have to be attributed to the entropy of the water molecules in contact with Ch.

Animations based on the simulation trajectories show that the Ch molecule lays flat on the water surface, with the two methyl groups M_1 and M_2 pointing outward. The alkane tail shows large amplitude oscillations, but no isomerization takes place around the $C_{17}-C_{20}$ bond and only a few around $C_{20}-C_{22}$. The configuration of the outer portion of the tail is also fairly constant, and relatively frequent isomerization events (once every ~50 ps, on average) occur only around the $C_{22}-C_{23}$ bond and, to a lesser extent, around $C_{23}-C_{24}$. Inspection of the Ch structure (see Figure 1), in fact, already suggests that rotations around $C_{22}-C_{23}$ can take place while keeping the main body and most of the tail in contact with the water surface; therefore, the rotation around this bond appears to be the torsional degree of freedom least affected by adsorption on water. As a comparison, we observe that the gas-phase molecule and a single Ch in bulk water at $T = 280$ K both display an isomerization rate of the alkane tail faster than that of Ch on water. Rotations around $C_{22}-C_{23}$ are favored in all cases, but only at the water surface do they become predominant, thus highlighting the effect of the surface environment on the intramolecular dynamics.

Absorption on water changes only slightly the average size and shape of Ch, similarly to what has been found for Ch in bulk water. The only noticeable difference between the two cases is that the narrowing of the probability distribution for the Ch principal momenta of inertia is more pronounced for Ch on water, probably because of the slower isomerization rate.

The analysis of simulation trajectories for the single Ch molecule on water shows that at any given time the probability to find the OH termination of cholesterol engaged in a HB as a donor is 51%, whereas the probability of receiving at least one (a)-bond is 76%. Not surprisingly, both probabilities are significantly lower than the corresponding values measured for Ch in water. Also in this case, only one accepting HB is present;

the probability of having two accepting bonds at the same time is less than 5%.

The real-time dynamics of the Ch−water hydrogen bonds, characterized by the same analysis applied in the case of cholesterol in water, shows that also for Ch on water the time dependence of the HB persistence function $P(t)$ (see previous subsection) is exponential both for accepting and donating bonds. In this case, the time constant τ_0 is 3.1 ps for donating bonds and is 4.6 ps for accepting bonds, that is, significantly less than in the case of cholesterol in water. Moreover, the difference between the two time constants for donating and accepting bonds shows that the free energy barrier for breaking a (d)-bond is 30% lower than the barrier to break (or form) an (a)-bond.[55]

The diffusion of amphiphilic molecules on water is often much faster than in water, mainly because mutual interactions and cage effects are weaker in the former than in the latter case. In this respect cholesterol is no exception, with an estimated diffusion constant of $D_{Ch}[n = 1] = 1.9 \pm 0.6 \times 10^{-5}$ cm^2/s, that is, at least 1 order of magnitude higher than in the case of diffusion in bulk water. Once again, the large error bar is mainly due to the fact that one is dealing with the properties of a single Ch molecule. In part, however, it is due to the fragile character of the cholesterol/water hydrogen bonding, reflected in the stick-and-slip motion of the Ch molecule, giving rise, in turn, to large fluctuations in the molecular mean square displacement even at long times t. The high value of the diffusion constant of Ch on water is highlighted by comparison with the diffusion constant of bulk water at the same temperature, that, despite a sizable size and mass advantage, is only 30% faster.[37]

The behavior of the Ch dipole moment on water is in many respects similar to that of Ch in water. Once again, the dipole length is nearly constant, and its direction shows fairly rapid fluctuations. The surface environment, however, breaks the isotropy of bulk absorption. As a result, the Ch dipole tends to lay in the surface plane (xy) with and average value $\langle |d_{xy}| \rangle = 4.98 \pm 0.02$ debye. The d_z component is smaller but not negligible, with an average value $|\langle d_z \rangle| = 1.72 \pm 0.04$ debye.[58] The direction of d_z points toward the water side of the interface, and therefore it follows the average polarization of the free water surface, as could be expected on the basis of electrostatics. However, the rapid time variations of the instantaneous dipole moment suggests that the dipolar energy cannot be a major factor for the stability and dynamics of Ch/water interfaces, at least for small Ch islands. The time dependence of the dipole autocorrelation function is similar to the one obtained for Ch in water. In particular, it is not exponential and displays at least two different time scales. The shortest one is comparable in the two cases, although the longest one is ~3 times longer for Ch in water than for Ch on water. These comparisons are consistent with the identification of the short time scale as due to vibrations, which are nearly unaffected by ab- and adsorption, whereas the long time scale is likely to be determined mainly by rotational diffusion, which is fastest for the adsorption case. The adsorption of the cholesterol changes the total surface polarization of water by 1.7 debye. The induced dipole points toward the vapor side of the interface and thus compensates almost exactly the d_z dipole of the adsorbed cholesterol.

Two cholesterol molecules on the water surface at $T = 280$ K condense into a bound pair, lying flat on the surface and keeping their long molecular axes nearly parallel. The dimer is always clearly bound, but the relative position of the two molecules is not rigidly defined and displays large amplitude variations over time. We even observe rare changes from the parallel to the antiparallel (like the one in Figure 6) configuration, taking place through a sudden transition. Also in this case the system has been equilibrated for 2 ns, and statistics have been gathered during a 8 ns simulation.

The Ch_2 adsorption energy is 42 ± 5 kcal/mol, or 21 ± 5 kcal/mol per Ch molecule, to be compared with the 14 ± 4 kcal/mol computed for the single Ch on water. Here and in what follows, the adsorption energy of the n-molecule cluster Ch_n is defined as:

$$E_{ads}[n] = -\{U[Ch_n \text{ on water}] - U[\text{water}] - nU[Ch]\} \quad (4)$$

where U[Ch] refers to the single gas-phase molecule, and U[water] is the average potential energy of a pure water slab with the same surface area of the [Ch_n on water] simulation. According to this definition, E_{ads} includes the cohesive energy of the cholesterol cluster. This last one may be isolated by defining two derived quantities, that is, E_{coh} and δE_{coh}, defined as follows:

$$E_{ccoh}[n] = E_{ads}[n] - nE_{ads}[1] \quad (5)$$

and

$$\delta E_{ads}[n] = E_{ads}[n] - E_{ads}[n-1] - E_{ads}[1] \quad (6)$$

The first of these quantities ($E_{coh}[n]$), in particular, measures the energy gain in condensing an n-molecule aggregate out of n isolated Ch adsorbed on water. The second one, that is, $\delta E_{ads}[n]$, measures the energy required to split an n-cluster into an $n - 1$ aggregate and a single Ch molecule, all species being adsorbed at the water surface. In the case of Ch_2, $E_{coh}[2] = \delta E_{ads}[2] = 15$ kcal/mol, showing that, unlike the bulk case, potential energy variations are sufficient to account for the remarkable stability of cholesterol aggregates adsorbed on water. The surface cohesive energy of this cluster, in particular, is comparable to the Ch_2 binding energy in the gas phase, also amounting to 15 kcal/mol.

The association of the two Ch molecules reduces their mobility, but it is still possible to estimate a diffusion constant $D_{Ch}[n = 2] = 1.2 \pm 0.210^{-5}$ cm^2/s, computed from the time dependence of the center of mass position of each molecule. Here and in what follows, the linear coefficient entering the determination of the diffusion coefficient is computed on the same $0.5 \leq t \leq 1$ ns time interval already used for both the absorbed and adsorbed monomer. This choice is motivated by our interest in quantifying the short time mobility of molecules, in order to probe the fluid-like character of cholesterol clusters on water. Much longer times would need to be considered for a fully quantitative determination of thermodynamic diffusion constants and, especially for larger clusters, to disentangle the effect of whole-cluster diffusion from the intracluster dynamics.

No Ch−Ch hydrogen bond is detected during the 2 ps of the statistics run, and the analysis of the water−Ch hydrogen bonding gives results very similar to those found in the single Ch on water case. The time constant t_0 for forming and breaking bonds rises slightly to 3.3 ps for donating HB, and to 5.3 for accepting bonds, probably because of the slower diffusion of Ch.

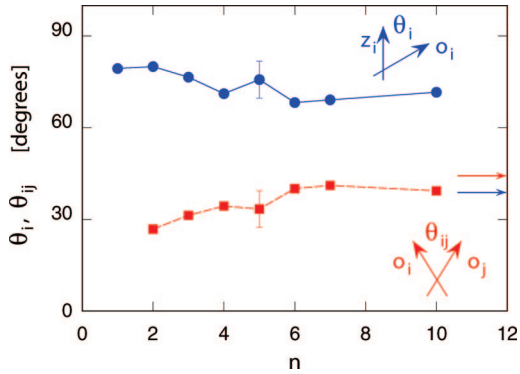

Figure 7. Full circles and blue line: size dependence of the average angle θ_z between the major cholesterol axis and the direction z normal to the surface. Full squares and red line: average value of the angle θ_{ij} between two Ch molecules in clusters of size n. The blue and red arrows point to the limiting values of θ_i and θ_{ij} for a full cholesterol monolayer on water, respectively. See text for the precise definition of θ_z and θ_{ij}. Representative error bars are shown.

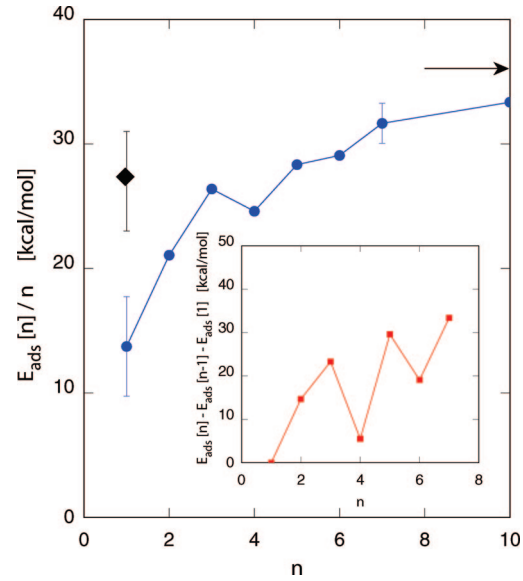

Figure 8. Adsorption energy per molecule $E_{ads}[n]/n$ as a function of cluster size n. The diamond at $n = 1$ corresponds to the absorption energy of a single Ch molecule in bulk water. The arrow marks the adsorption energy per molecule at monolayer coverage. Inset: energy required to split an $[n]$ cluster into an $[n - 1]$ aggregate and a single Ch molecule adsorbed on water. Representative error bars are shown.

The molecular association slows down significantly the rotational and isomerization dynamics, as reflected in the time evolution of the molecular dipoles. Once again the time autocorrelation function of the molecular dipole is the superposition of two exponential decays. The shortest time scale is the same for Ch and Ch_2, but the time constant of the slowest process is more than two times longer than the slowest relaxation time for the single Ch molecule on water. The time-dependent properties are reflected in the average value of the dipole moment and its d_{xy} and d_z components. Individual molecules carry a dipole whose average length is 5.56 ± 0.01 debye, which is not much different from that of gas-phase Ch in its ground state. The average dipole of the adsorbed dimer is 6.50 ± 0.02 debye, which is intermediate between the dipole of the cholesterol dimer in the parallel ($\sim$10) and antiparallel ($\sim$0 debye) configuration. Also in this case, the cluster dipole tends to lie in the xy plane with, however, an average $|\langle d_z \rangle|$ component of 1.72 ± 0.03 debye per molecule, still pointing toward the water side of the interface (i.e., $\langle d_z \rangle = -1.72 \pm 0.03$ debye, in our convention). At the same time, the dipole moment of the water surface changes by $\delta d_z^w = +1.20 \pm 0.05$ debye per cholesterol molecule, thus substantially reducing the net polarization of the interface.

D. Small Cholesterol Islands on Water. Computations for islands of up to 10 Ch molecules adsorbed on water reveal the same qualitative features and trends already found for the two smallest (Ch and Ch_2) clusters. In all these cases, molecules tend to lay flat on the water surface and form condensed aggregates of apparent 2D character, even though, starting from $n = 4$, slight but increasing deviations from planarity are observed with increasing cluster size. These are predominantly caused by the occasional stacking of cholesterol pairs joined by their flat α-side and arranged in such a way that both the long molecular axes and the polycycle plane are orthogonal to the water surface. The predominantly planar character of adsorbed clusters can be quantified by computing the average value of the angles $[\theta_i, i = 1,..., n]$ between the $\hat{z}$ axis and the vector $\hat{o}_i$ pointing from C_3 to C_{17} (labels refer to (Figure 2) of molecule i, and thus approximately oriented along the major molecular axis. The results are collected in Figure 7. Clusters are confined to a single simulation cell up to and including $n = 7$, whereas structures extending across the entire simulation cell are observed for $n = 10$. In all cases, coverage is far below the monolayer coverage, with the $n = 10$ cluster corresponding to only 25% of the full monolayer coverage measured in ref 19. As a consequence, the lateral pressure on the cholesterol adsorbate is negligible, and the slight deviations from planarity observed for $n \geq 4$ are apparently due to stronger Ch−Ch attractive forces, whereas the transition to the up-right configuration typical of Langmuir layers (main transition, see ref 1) takes place at significantly higher coverage because of repulsive interactions.

The structure of the islands appears to be fluid-like, with slow but apparent fluctuations in shape. In all cases, molecules tend to align their major axis along a common direction that, however, changes over time. The remarkable alignment of molecules can be monitored by computing the average of $|\hat{o}_i \cdot \hat{o}_j|$, where $\hat{o}_i$ and $\hat{o}_j$ are the unit vectors defined above for molecules i and j, respectively. The average value of $\chi_2 = 2_{i<j}|\hat{o}_i \cdot \hat{o}_j|/n(n - 1)$, computed on all the $n \times (n - 1)/2$ Ch pairs in the clusters is shown in Figure 7. Deviations from a near-parallel orientation are slight, and the common alignment of all molecules in the cluster, irrespective of their distance, somehow anticipates the liquid crystal nature of bulk cholesterol.

Despite the high mobility of cholesterol in aggregates of up to $n = 10$ molecules, no fragmentation (fission) of islands, nor separation (evaporation) of single molecules, onto the surface takes place during our simulations, lasting at least 5 ns after a 2 ns equilibration time. This observation emphasizes the remarkable cohesiveness of these aggregates. Needless to say, this last statement is valid only for the microscopic/mesoscopic times covered by the simulation or for the low but nonvanishing coverages of our finite samples, since finite clusters on an extended surface are by definition metastable at any nonvanishing temperature. Nevertheless, the long lifetime of even the smallest clusters shows that at $T = 280$ K cholesterol aggregation is a spontaneous process for any overlayer of nonvanishing concentration.

The dependence of the adsorption energy per molecule $E_{ads}(n)$ on the cluster size n is displayed in Figure 8, where an arrow marks the limiting value for the ordered monolayer computed by relaxing the geometry suggested in ref 19 using the same

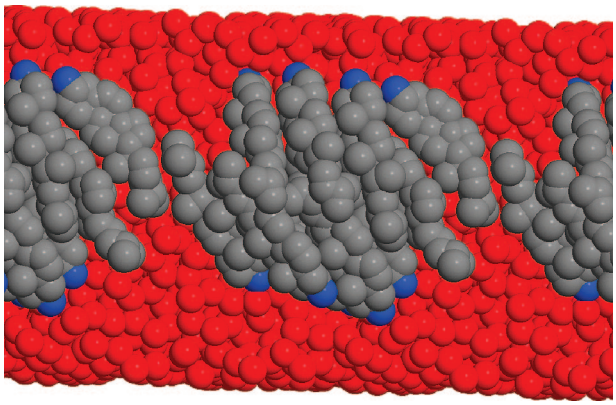

Figure 9. Snapshot of the $n = 10$ cholesterol cluster adsorbed on water. The simulation cell has been replicated two times along the y direction. Red atoms: water oxygen; black atoms: cholesterol carbon; blue atoms: cholesterol oxygen. Hydrogen atoms are not shown.

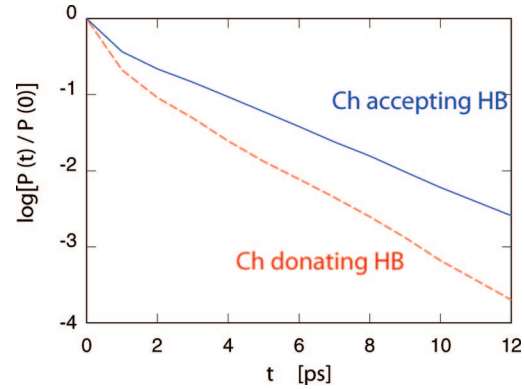

Figure 10. Persistence probability function $P(t)$ for hydrogen bonds (see text) computed for Ch_3 on water.

potential employed here for the adsorbed clusters. Starting from the fairly low value estimated for a single Ch on water, E_{ads} quickly saturates to a value close to 30 kcal/mol, thus suggesting that Ch−Ch interactions are short-range, including those mediated by the water substrate. We emphasize once again that, according to our definition, E_{ads} includes the Ch−Ch cohesive energy. Slight deviations from a monotonic size dependence are apparent in Figure 8, whose amplitude is comparable and sometimes larger than the estimated error bar. The meaning of these slight anomalies becomes more apparent if we consider the derived energies defined above. Both $E_{coh}[n]$ and $\delta E_{ads}[n]$ (this last shown in the inset of Figure 8) display clear peaks at $n = 3$, 5, and 7, and dips at $n = 4$ and 6. The peaks point to particularly stable aggregates, analogous to the magic clusters often found in the size distribution of atomic clusters.[59] On the other hand, dips in $\delta E_{ads}[n]$ might correspond to rate limiting steps in the growth of cholesterol aggregates from single molecule addition. In the case of both peaks and dips, it is difficult to predict their special character from a simple visual inspection of their structures. Apart from the $n = 2$ case, it is in fact difficult to identify clear geometries for these fluid-like, 2D aggregates, and none seems to suggest a particularly efficient packing of molecules on the water surface. The $n = 7$ cluster, for instance, which could have been expected to adopt a compact centered-hexagonal geometry with all molecules in the upright orientation, is invariably found in a 2D, translationally disordered configuration. The slight increase of E_{ads} from $n = 7$ to $n = 10$ might be due to the fact that the $n = 10$ cluster extends across the entire simulation cell, giving rise to an extended stripe in the periodically repeated system and reducing slightly the cluster contour per molecule. We observe, however, that the contour of the $n = 10$ cluster is fairly rough and changes rapidly in time, pointing to a relatively low line tension. The similarity of E_{ads} for $n = 10$ with the monolayer value is probably a coincidence, since the Ch configuration is very different in the two cases. In the $n = 10$ cluster, in fact, molecules tend to lay flat on the water surface, whereas they adopt an upright geometry with only their OH termination in contact with water in the monolayer case. Nevertheless, we note that cholesterol molecules in the $n = 10$ cluster tend to adopt a remarkable configuration reminiscent of a 1D version of the familiar lipid bilayer structure. In these configurations (see Figure 9), molecules are arranged along two adjacent lines, the alkane tails are confined in the inner portion of the stripe, the OH groups point toward the free water surface, and the cholesterol long axes are aligned.

For all clusters up to $n = 10$, hydrogen bonding takes place preferentially with water, and the time scales for forming and breaking bonds depend only weakly on the island size. The time dependence of the persistence probability $P(t)$ defined in Section IIIB appears to be exponential in all cases, as shown in Figure 10 for the $n = 3$ island. Once again, the slight anomaly at times shorter than 1 ps might be a consequence of our smoothing of the high frequency vibrations of the OH bond. Ch−Ch hydrogen bonding starts to appear in the $n = 3$ islands, but up to $n = 10$ its probability is low, and the time constant τ_0 for Ch−Ch hydrogen bond formation and breaking is short ($\tau_0 \approx 1$ ps). The marginal probability of Ch−Ch hydrogen bonding could have been expected, since the typical cluster configurations, in which cholesterol molecules lay flat on the water surface exposing their M_1 and M_2 methyl groups to the vapor side do not favor the close proximity of their OH terminations to within ~3.5 Å.

As expected, the diffusion of cholesterol molecules tends to decrease with increasing cluster size, thus making more difficult the determination of their diffusion constant by MD. On the other hand, fluctuations in the average displacement are reduced by averaging over an increasing number of Ch molecules. As a result, in all cases we are able to observe a clear linear range in the average mean square displacement $d_n^2(\tau) = \sum_{i=1}^{n} \langle |R_{CM}^{(i)}(t+\tau) - R_{CM}^{(i)}(t)|^2 \rangle_t / n$ versus t (see Figure 11), and the relative (statistical) error on the diffusion constant does not rise dramatically with increasing cluster size up to $n = 7$, even though for all clusters we consider the same time interval $0.25 \leq t \leq 0.5$ ns for the computation of $D_{Ch}[n]$. The diffusion constant drops below the error bar for $n = 10$, perhaps because of the different Ch configuration (extended stripe instead of a confined island) adopted by this sample, which reduces the contour length and slightly increases packing and cohesion. The simulation results for the size dependence of the diffusion constant are collected in the inset of Figure 11. As already pointed out before, the relatively short simulation times used in our study imply that the computed mean square displacement reflects both the contributions of the intracluster dynamics and of the whole-cluster diffusion.[60]

Computer simulations for water solutions of protein and organic micelles have shown that water molecules in the first hydration layer display a characteristically slow dynamics, whose time scale increases with increasing hydrophilic character of the guest species.[57] We attempted a similar analysis for the adsorbed Ch aggregates by first identifying the water molecules whose distance from any cholesterol molecule was less than a preassigned value ($R_c = 4$ Å for the water oxygen−cholesterol CM distance) and then computing the time dependence of mean

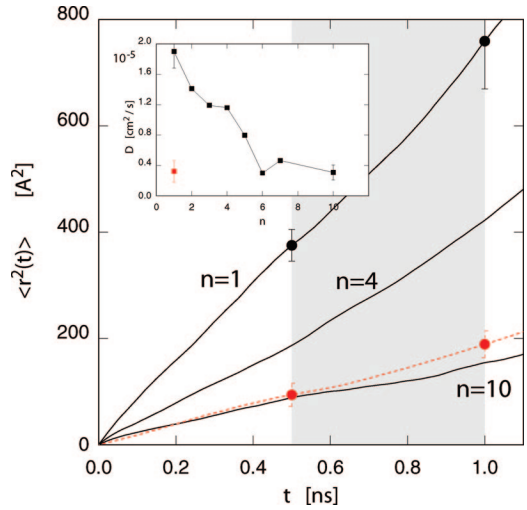

Figure 11. Mean square displacement of cholesterol molecules on the water surface in clusters of size $n = 1$, 4, and 10. The mean square displacement of a single Ch molecule in bulk water (dotted line) is shown for a comparison. Inset: size dependence of the diffusion coefficient of cholesterol molecules on water. D_n is computed from the linear part of the molecular mean square displacement for $0.5 \leq t \leq 1$ ns (shaded area in the main picture). Representative error bars are shown.

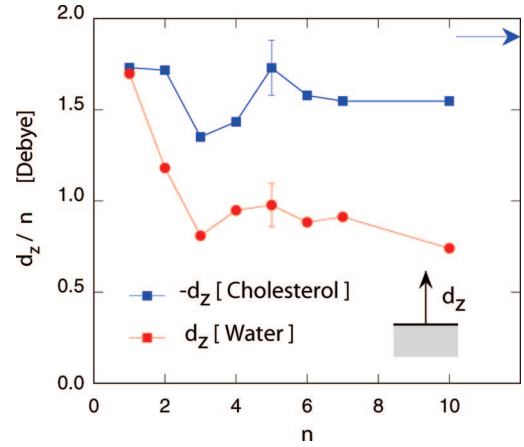

Figure 12. Filled squares and blue line: size dependence of the average electrostatic dipole moment of adsorbed Ch clusters divided by the number of adsorbed molecules. Filled circles and red line: average electrostatic dipole polarization of the water surface (per Ch molecule) induced by the adsorption of cholesterol clusters. In both cases $\langle d \rangle = d_z$ because of in-plane symmetry. The blue arrow marks the dipole moment per Ch molecule in the full monolayer on water computed at $T = 280$ K. The corresponding change of the water polarization is negative. Representative error bars are shown.

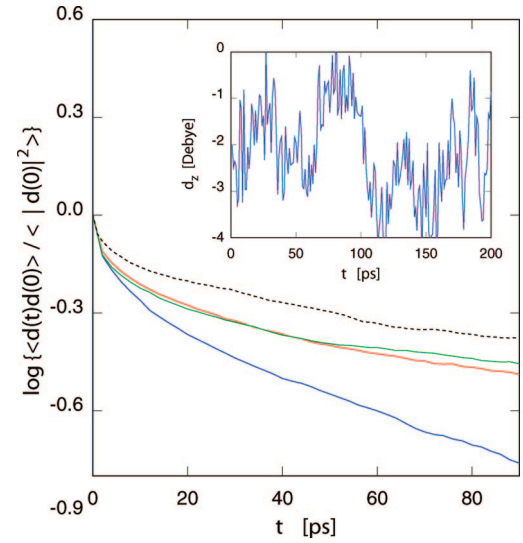

Figure 13. Time autocorrelation function for the molecular dipole of cholesterol in clusters of size $n = 1$ (blue curve), $n = 2$ (red), and $n = 3$ (green). The same function for a single cholesterol molecule absorbed in bulk water is shown for a comparison (black dotted line).

square displacement of the tagged water molecules, irrespective of their distance from the cholesterol islands at later times. Unfortunately, and despite extensive averaging over different starting times, the deviations of mobility with respect to bulk and surface water turn out to be at the limit of statistical significance, probably because of the small size of the cholesterol clusters, reflected in a correspondingly small number of neighboring water molecules. However, the trend suggested by the simulation results points to an enhanced mobility of the water molecules in direct contact with Ch, consistent with the predominantly hydrophobic character of the interface. The result might be different and possibly stronger at full monolayer coverage, when the water cholesterol contact occurs at the hydrophilic apex of cholesterol.

The size dependence of the electrostatic dipole moment of individual Ch molecules and of whole Ch adsorbed clusters is fairly regular, and a few general trends and properties emerge clearly from the simulation results. Each molecule carries a dipole whose modulus is nearly constant at $|d| = 5.5$ debye, and the combination of dipole from individual molecules gives rise to a cluster dipole predominantly lying in the xy plane, whose average modulus tends to grow (although not monotonically) with increasing cluster size, thus pointing to an incipient 2D ferro-electricity of Ch on water. The force driving the dipoles' alignment is unlikely to be of electrostatic origin and has to be attributed to the steric interactions that give rise to the parallel arrangement of molecules along their major molecular axis. Electrostatic forces, however, might become important for much larger islands, possibly giving rise to different polarization domains. The z-component of the cluster dipole is always directed toward the water slab, and its size grows regularly and fairly rapidly with increasing n. The variation of the surface water polarization tends to compensate the rise of the d_z cluster dipole. The simulation results up to $n = 10$ are summarized in Figure 12. The time autocorrelation function of the cholesterol molecular dipole shows a nonexponential decay for all cluster sizes. Moreover, as can be verified in Figure 13, the dependence of this function on time is remarkably insensitive to cluster size as soon as $n > 1$. The association of cholesterol in cluster of nearly parallel molecular direction apparently determines the rate of the rotation and isomerization processes causing the relaxation of the molecular dipole.

The effect of Ch adsorption on the surface free energy has been estimated by computing the surface tension of the composite (water + Ch island) surface and comparing it with that of the clean water surface. Given the heterogeneous nature of the Ch/water surface, our computation cannot provide a rigorous characterization of the surface free energy, nor we can unambiguously split the free energy variations into water and cholesterol contributions. Nevertheless, the results, collected in Figure 14, clearly show that low coverage adsorption of Ch has little effect on the surface free energy. We anticipate that the picture changes drastically at higher coverage, when the increase in the lateral pressure pushes molecules against each other, forcing them into an upright configuration and decreasing

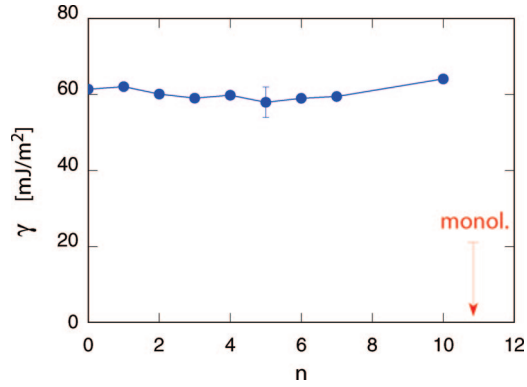

Figure 14. Surface tension γ for the composite surface made of a cholesterol island adsorbed on the water surface of fixed area $A = 1525$ Å^2. The surface tension of the interface at full monolayer coverage (shown by the vertical arrow) vanishes to within the simulation error bar. Representative error bars are shown.

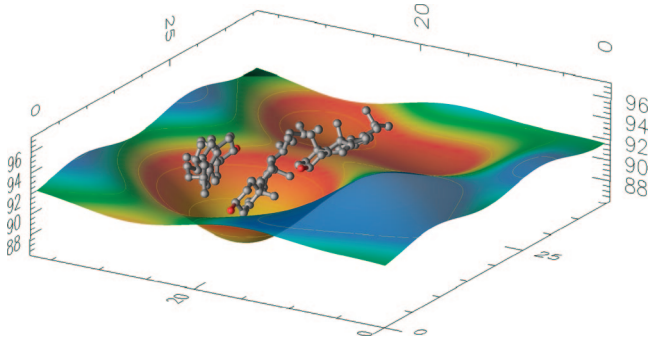

Figure 15. Geometric representation of the water surface underlying a Ch_3 island. Instantaneous snapshot from a nanosecond simulation at $T = 280$ K.

the surface tension to virtually zero. The slight effect of Ch adsorption on the surface tension implies that only minor changes can be expected in the dynamics of capillary waves of the surface. Cholesterol islands, however, tend to penetrate somewhat into the surrounding water, giving rise to an apparent quasistatic deformation of the water surface, as shown in Figure 15 for the Ch_3 cluster. The position of the water surface has been located using a method similar to the one used in ref 61. We characterize the surface indentation as quasistatic because it appears to be nearly constant in shape and size, but it evolves in time following the diffusion of the Ch island on the water surface.

IV. Summary and Conclusions

Molecular dynamics simulations of small cholesterol clusters Ch_n floating on water provide a direct and intriguing view of the early stages of aggregation for this prototypical amphiphilic lipid, which plays a major role in biological systems and in biomaterials.

Up to the sizes considered in our study ($n = 10$), cholesterol forms 2D fluid-like islands that, despite the inherent metastability of finite aggregates on extended surfaces, strictly retain their integrity over the mesoscopic times of our simulations. Cholesterol molecules, in particular, tend to lie flat on the water surface, exposing their M_1 and M_2 groups to the vapor side, and align their longest axis along a common direction. The fluid character is highlighted by the computation of the molecular mean square displacement as a function of time t, which on the nanosecond time scale and irrespective of cluster size, displays a clear linear growth with increasing t. Up to $n = 7$, the slope of the linear term corresponds to a diffusion constant of $\sim 10^{-5}$ cm^2/s, not far below that of liquid water at ambient conditions. On longer time scales, the finite size of clusters will affect the growth of the molecular mean square displacement, progressively reducing it to the much slower pace of whole-cluster diffusion, which is expected to scale as $1/\sqrt{n}$ with increasing cluster size. These structural and dynamical properties somehow anticipate the liquid crystal character of bulk cholesterol. At higher coverage, when the cholesterol film becomes homogeneous, the system will make a transition to a different liquid crystal phase, in which molecules adopt an upright configuration.

The adsorption energies of the single Ch molecule and dimer Ch_2 on water are much less than the absorption energy of the same species in bulk water. However, both species float on the water surface, and in no case do we observe a cholesterol molecule or larger aggregate dipping below the surface. These results imply that entropy plays an important role in localizing cholesterol at the surface, and thus is at the origin of its amphiphilic character. Moreover, the analysis of the different entropy contributions shows that neither translational nor vibrational entropy of cholesterol can account for its marked preference for adsorption on water with respect to bulk absorption. The missing entropy contribution, therefore, has to be attributed to changes in the water configuration and dynamics in the vicinity of the cholesterol aggregate.

Entropy plays a role also in the aggregation of the smallest cholesterol clusters in and on water. Potential energy rises by 20 kcal/mol when Ch_2 is formed in bulk water out of two absorbed cholesterol molecules. The potential energy gain in adding one Ch unit to Ch_3 floating on water is marginal at best. The same is true in going from $n = 5$ to $n = 6$. Nevertheless, all clusters appear to be stable during simulations lasting many nanoseconds, emphasizing the role of entropy contributions in stabilizing these species in a water environment. Beyond the very small sizes ($n \leq 6$), however, potential energy emerges as the most important force driving the aggregation of adsorbed cholesterol molecules, and the adsorption energy per molecule converges quickly to the monolayer limit. This observation suggests that the direct and water-mediated Ch−Ch interaction is short-range.

The investigation of the water surrounding the hydrocarbon body of cholesterol reveals features characteristic of hydrophobic interfaces. The water density is greatly reduced over a fairly thick layer around cholesterol, large and rapid density fluctuations are apparent, and the mobility of water molecules seems to be enhanced. Cholesterol, in particular, gives rise to an apparent indentation of the water surface. The stabilization of this large amplitude modulation in the vicinity of adsorbed cholesterol islands anticipates the dramatic enhancement of fluctuations in the water surface revealed in ref 62. The surface tension of the composite interface, however, displays only slight changes with respect to the pure water surface, consistent with the fact that the lateral pressure is vanishingly small for incomplete layers.

The dipole moment of individual molecules has nearly constant length, but its orientation displays fairly rapid (~2 ps) variations due to vibrations, whereas occasional isomerization events and molecular rotations change its direction on a longer (1 ns) time scale. The superposition of relaxation channels of different characteristic time gives rise to a nonexponential decay of the dipole time-autocorrelation function.

The hydrogen bonding, which is expected to play a major role in the monolayer case and even more for bilayers in water, provides only ~30% of the adsorption potential energy. Moreover, hydrogen bonding takes place almost exclusively between cholesterol and water, whereas Ch−Ch HBs, which represent a major structural motif in solid cholesterol phases, are very rare in adsorbed clusters.

Because of the limited cross section of our water slab, the $n = 10$ cluster, corresponding to 25% of a monolayer coverage, stretches across the entire simulation cell, giving rise to extended stripe-like structures. Large fluctuations in the stripes' contour suggest that the line tension of dilute cholesterol layers on water is modest, even though its precise value cannot be estimated with any confidence by our simulations.

In conclusion, the results of our simulations provide a quantitative basis for coarse graining models of cholesterol on water[21] and for the kinetic modeling of aggregation in dilute cholesterol overlayers. The low-coverage range analyzed in our study is difficult to investigate by experimental means. Simulation, therefore, provides the most suitable alternative to visualize and quantify the properties of these systems.

The validity and reliability of simulation results depend on the quality of the underlying potential model. Not unexpectedly, we found that the cross interaction of water and cholesterol is the most uncertain ingredient of our simulation, especially for what concerns the dispersion (van der Waals) part. Moreover, as already pointed out in several simulation papers, the usage of rigid ion models might severely limit the accuracy and reliability of simulation results for highly inhomogeneous systems such as water−organic interfaces. Despite, or perhaps because of these uncertainties, our exploration of low-coverage cholesterol overlayers on water may provide additional motivations for further investigations of these simple yet important systems.

Supporting Information Available: This material is available free of charge via the Internet at http://pubs.acs.org.

References and Notes

(1) Kaganer, V. M.; Möhwald, H.; Dutta, P. *Rev. Mod. Phys.* **1999**, *71*, 779–819.

(2) Petty, M. C. *Langmuir-Blodgett Films: An Introduction*; Cambridge University Press: Cambridge, 1996.

(3) Safran, S. A. *Statistical Thermodynamics of Surfaces, Interfaces, and Membranes*; Addison-Wesley: Reading, MA, 1994.

(4) Alberts, B.; Johnson, A.; Lewis, J.; Raff, M.; Roberts, K.; Walter, P. *Molecular Biology of the Cell*, 4th ed.; Garland Science: New York, 2002.

(5) Stryer, L. *Biochemistry*, 4th ed.; Freeman, New York, 1995.

(6) Langmuir, I. *J. Am. Chem. Soc.* **1917**, *39*, 1848–1906.

(7) Ligler, F. S.; Sapsford, K. E.; Golden, J. P.; Shriver-Lake, L. C.; Taitt, C. R.; Dyer, M. A.; Barone, M. A.; Myatt, C. J. *Anal. Sci.* **2007**, *23*, 5–10.

(8) (a) Cracknell, J. A.; Vincent, K. A.; Armstrong, F. A. *Chem. Rev.* **2008**, *108*, 2439–2461. (b) Bullena, R. A.; Arnotb, T. C.; Lakemanc, J. B.; Walsh, F. C. *Biosens. Bioelectron.* **2006**, *21*, 2015–2045.

(9) (a) Patti, J. T.; Montemagno, C. D. *Nanotechnology* **2007**, *18*, 325103. (b) Xi, J. Z.; Ho, D.; Chu, B.; Montemagno, C. D. *Adv. Funct. Mater.* **2005**, *15*, 1233–1240.

(10) (a) Scott, H. L. *Curr. Opin. Struct. Bio.* **2002**, *12*, 495–502. (b) Müller, M.; Katsov, K.; Schick, M. *Phys. Reports* **2006**, *434*, 113–176.

(11) Venturoli, M.; Sperotto, M. M.; Kranenburg, M.; Smit, B. *Phys. Reports* **2006**, *437*, 1–54.

(12) Hsu, L.-Y.; Kampf, J. W.; Nordman, C. E. *Acta Cryst. B* **2002**, *58*, 260–264.

(13) Craven, B. M. *Nature* **1976**, *260*, 727–729.

(14) Bogren, H.; Larsson, K. *Biochim. Biophys. Acta* **1963**, *75*, 65–69.

(15) Bloom, M.; Evans, E.; Mouritsen, O. G. *Q. Rev. Biophys.* **1991**, *24*, 293–397.

(16) (a) Brown, D.; London, E. *J. Membr. Biol.* **1998**, *164*, 103–114. (b) Simons, K.; Ikonen, E. *Nature* **1997**, *387*, 569–572.

(17) Harroun, T. A.; Katsaras, J.; Wassall, S. R. *Biochemistry* **2006**, *45*, 1227–1233.

(18) Harroun, T. A.; Katsaras, J.; Wassall, S. R. *Biochemistry* **2008**, *47*, 7090–7096.

(19) (a) Solomonov, I.; Weygand, M. J.; Kjaer, K.; Rapaport, H.; Leiserowitz, L. *Biophys. J.* **2005**, *88*, 1809–1817. (b) Rapaport, H.; Kuzmenko, I.; Lafont, S.; Kjaer, K.; Howes, P. B.; Als-Nielsen, J. *Biophys. J.* **2001**, *81*, 2729–2736. (c) Lafont, S.; Rapaport, H.; Sömjen, G. J.; Renault, A.; Howes, P. B.; Kjaer, K.; Als-Nielsen, J.; Leiserowitz, L.; Lahav, M. *J. Phys. Chem. B* **1998**, *102*, 761–765, See also ref 20.

(20) Kuzmenko, I.; Rapaport, H.; Kjaer, K.; Als-Nielsen, J.; Weissbuch, I.; Lahav, M.; Leiserowitz, L. *Chem. Rev.* **2001**, *101*, 1659–1696.

(21) Noid, W. G.; Chu, J.-W.; Ayton, G. S.; Krishna, V.; Izvekov, S.; Voth, G. A.; Das, A.; Andersen, H. C. *J. Chem. Phys.* **2008**, *128*, 244114.

(22) van Miltenburg, J. C.; van Genderen, A. C. G.; van den Berg, G. J. K. *Thermochim. Acta* **1998**, *319*, 151–162.

(23) (a) Jorgensen, W. L.; Maxwell, D. S.; Tirado-Rives, J. *J. Am. Chem. Soc.* **1996**, *118*, 11225–11236. (b) Kaminski, G.; Jorgensen, W. L. *J. Phys. Chem.* **1996**, *100*, 18010–18013.

(24) Head-Gordon, T.; Hura, G. *Chem. Rev.* **2002**, *102*, 2651–2670.

(25) Javed, A.; Akram, M.; Shafiq, M. I. *Rom. Journ. Phys.* **2006**, *51*, 819–826.

(26) (a) Perdew, J. P.; Burke, K.; Ernzerhof, M. *Phys. Rev. Lett.* **1996**, *77*, 3865–3868. (b) *ibid.* **1997**, *78*, 1396(E).

(27) Soler, J. M.; Artacho, E.; Gale, J. D.; García, A.; Junquera, J.; Ordejón, P.; Sánchez-Portal, D. *J. Phys.: Condens. Matter* **2002**, *14*, 2745–2779.

(28) (a) Cournia, Z.; Vaiana, A. C.; Ullmann, G. M.; Smith, J. C. *Pure Appl. Chem.* **2004**, *76*, 189–196. (b) Cournia, Z.; Smith, J. C.; Ullmann, G. M. *J. Comput. Chem.* **2005**, *26*, 1383–1399.

(29) Weiner, S. J.; Kollman, P. A.; Case, D. A.; Singh, U. C.; Alagona, G.; Profeta, S., Jr.; Weiner, P. *J. Am. Chem. Soc.* **1984**, *106*, 765–784.

(30) Smith, W.; Leslie, M.; Forester, T. R.; *DL-POLY, Version 2.14*; Daresbury Laboratories: Daresbury, Warrington, UK, 2003.

(31) Chen, B.; Siepmann, J. I. *J. Phys. Chem. B* **1999**, *103*, 5370–5379.

(32) Voth, G. A.; Wu, Y.; Tepper, H. L. *J. Chem. Phys.* **2006**, *124*, 024503.

(33) Popular DF approximations do not include dispersion interactions. Perturbative methods such as MP2 are very time consuming for molecules larger that 15−20 atoms, and their quality tends to degrade with increasing system size.

(34) Santra, B.; Michaelides, A.; Scheffler, M. *J. Chem. Phys.* **2007**, *127*, 184104.

(35) (a) Curtiss, L. A.; Frurip, D. J.; Blander, M. *J. Chem. Phys.* **1979**, *71*, 2703–2711. See also (b) Mas, E. M.; Bukowski, R.; Szalewicz, K.; Groenenboom, G. C.; Wormer, P. E. S.; van der Avoird, A. *J. Chem. Phys.* **2000**, *113*, 6687–6701.

(36) Zimdars, D.; Dadap, J. I.; Eisenthal, K. B.; Heinz, T. F. *J. Phys. Chem. B* **1999**, *103*, 3425–3433.

(37) $D_w = 2.32 \pm 0.05 \times 10^{-5}$ cm^2/s, computed for the SPC/Fw model in ref 32, which is in close agreement with the experimental value $D_w = 2.3 \times 10^{-5}$ cm^2/s; see ref 38.

(38) Krynicki, K.; Green, C. D.; Sawyer, D. W. *Faraday Discuss. Chem. Soc.* **1978**, *66*, 199–208.

(39) Rowlinson, J. S.; Widom, B. *Molecular Theory of Capillarity*; Oxford University Press: Oxford, 1982.

(40) (a) Chen, F.; Smith, P. E. *J. Chem. Phys.* **2007**, *126*, 221101. (b) Vega, C.; de Miguel, E. *J. Chem. Phys.* **2007**, *126*, 154707.

(41) *Handbook of Chemistry and Physics*; CRC: Boca Raton, FL, 1986.

(42) The low value of the surface polarization makes it sensitive to the precise procedure adopted to measure it. The value reported in the present paper has been computed by first dividing the N_w molecules in each simulation frame into an upper and a lower half-slab, according to the z-coordinate of the oxygen atoms. Then, the average surface polarization is defined as the average dipole moment per unit area of each of the two water half-slabs. Changes in the surface polarization due to cholesterol adsorption are far less sensitive to the precise definition.

(43) Kralchevsky, P. A.; Kuniaki Nagayama, K. *Adv. Colloid Interface Sci.* **2000**, *85*, 145–192.

(44) Haberland, M. E.; Reynolds, J. A. *Proc. Nat. Acad. Sci. USA* **1973**, *70*, 2313–2316.

(45) Saad, H. Y.; Higuchi, W. I. J. *Pharm. Sci.* **1965**, *54*, 1205–1206.

(46) Finney, J. *NATO Sci. Ser. Ser. A. Life Sci.* **1999**, *305*, 115–124.

(47) van Oss, C. J. *J. Mol.* **2003**, *16*, 177–190.

(48) Paulaitis, M. E.; Garde, S.; Ashbaugh, H. S. *Curr. Opin. Colloid Interface Sci.* **1996**, *1*, 376–383.

(49) (a) Scheraga, H. A. *Biomol. Struct. Dyn.* **1998**, *16*, 447–460. (b) Southall, N. T.; Dill, K. A.; Haymet, A. D. J. *J. Phys. Chem. B* **2002**, *106*, 521–533.

(50) Dispersion and Coulomb energies include the contributions from hydrogen bonding, which in our description results from a combination of charges and LJ parameters for oxygen and hydrogen atoms.

(51) Chandler, D. *Nature* **2007**, *437*, 640, and references therein.
(52) Paschek, D.; Köddermann, T.; Ludwig, R. *Phys. Rev. Lett.* **2008**, *100*, 115901.
(53) Luzar, A. *J. Chem. Phys.* **2000**, *113*, 10663.
(54) Hammerich, A. D.; Buch, V. *J. Chem. Phys.* **2008**, *128*, 111101.
(55) We are implicitly assuming an Arrhenius behaviour, with the same pre-exponential factor for accepting and donating bonds.
(56) Keutsch, F. N.; Fellers, R. S.; Brown, M. G.; Viant, M. R.; Petersen, P. B.; Saykally, R. J. *J. Am. Chem. Soc.* **2001**, *123*, 5938–5941.
(57) (a) See, for instance Pizzitutti, F.; Marchi, M.; Sterpone, F.; Rossky, P. J. *J. Phys. Chem. B* **2007**, *111*, 7584–7590. (b) Sterpone, F.; Marchetti, G.; Pierleoni, C.; Marchi, M. *J. Phys. Chem. B* **2006**, *110*, 11504–11510.
(58) Note that in the case of the planar component we quote the average of an absolute value, whereas in the case of the *z*-component we quote the absolute value of the average.
(59) Doye, J. P. K.; Wales, D. J. *Phys. Rev. Lett.* **2001**, *86*, 5719–5722.
(60) This last contribution could be estimated by computing the mean square displacement of the cluster CM. For $n \geq 4$, however, the error bar on the data is comparable to their average value.
(61) Bresme, F.; Chacón, E.; Tarazona, P. *Phys. Chem. Chem. Phys.* **2008**, *10*, 4704–4715.
(62) Datta, A.; Kundu, S.; Sanyal, M. K.; Daillant, J.; Luzet, D.; Blot, C.; Struth, B. *Phys. Rev. E* **2005**, *71*, 041604.

JP8084759